Optoelectronic Properties and Raman Spectra of Layered $TaWSe_2$ Ternary Alloys

By

Xin Sun

Thesis

Submitted to the Faculty of the

Graduate School of Vanderbilt University

in partial fulfillment of the requirements

for the degree of

MASTER OF SCIENCE

In

Electrical Engineering

August 13, 2021

Nashville, Tennessee

Approved :

Yaqiong Xu, Ph.D.

Enxia Zhang, Ph.D.

TABLE OF CONTENTS

Page

LIST OF FIGURES

Figure **Page**

Chapter I. Introduction

1. Development and application of traditional 2D material

Two-dimensional (2D) materials have been studied theoretically by researchers for over 150 years [1]. Recently, the scientific community has started to experimentally realize the actual properties of these materials for advanced applications [2]. In 2004, Geim and Novoselov successfully isolated a stable single-layer allotrope of carbon: graphene [3]. This fantastic outcome has motivated many researchers to focus on graphene. They have found that graphene shows many unique properties, which can be applied to several areas like chemistry, electronics, optics, and many others [4]–[6]. With successful research results on graphene, researchers also put eyes on other 2D materials. Beyond graphene, a broad spectrum of 2D materials possesses various electronic properties ranging from insulators to semiconductors to metals and even superconductors. One of the most studied traditional 2D material families is transition metal dichalcogenides (TMDC). TMDC materials have a general structure of MX_2 where M is a transition metal from group IV, V, or VI and X is a chalcogen atom, like MoS_2 and WSe_2 [7]. Since TMDC materials contain several elements and layer dependent properties, TMDC materials can present varied electrical, optical, and chemical properties [8]–[10]. Two distinctive features of TMDCs are strong excitonic effects and valley/spin-dependent properties. Some TMDCs, like MoS_2, possess indirect bandgaps for bulk crystals but become direct-bandgap semiconductors in their atomic layer form [11]. Moreover, the broken in-plane inversion symmetry in the monolayer limit often gives rise to valley-dependent optical and electrical properties [12].

Graphene analogues are another important type of 2D material. These include hexagonal boron nitride (hBN), black phosphorus (BP), and a recent addition, borophene [13]–[16]. hBN is an insulator with an ultra-flat surface and highly stable structure. It can be used as a substrate for other 2D materials due to the reduced coulomb scattering and excellent interface properties as well as a passivation layer to protect the materials from doping, oxidation, and degradation [17]. Black phosphorus has much stronger layer-to-layer interaction than layered semiconducting TMDCs, leading to a stronger thickness dependence of its bandgap, from about 0.33 eV in bulk to 2.0 eV in monolayer [18]. It also exhibits higher carrier mobility than many semiconducting TMDCs. Thin-film BP has shown strong interaction with light making it promising for various electronic and photonic applications [19], [20]. Borophene is highly flexible that can be widely used in fabricating flexible nanodevices. Furthermore, the anisotropic structure in borophene can result in directional magnetic and electronic properties, which can be used for multiple applications [21]–[23]. Another prominent category of 2D materials is transition metal oxides, including titania- and perovskite-oxides. Those oxide nanosheets have exhibited great potential for new capacitors and energy-storage devices [24].

Compared with traditional 3D materials, 2D materials provide an enormous opportunity to study light absorption and emission in atomic layers. Also, the strong optoelectronic properties of many 2D materials can contribute to realizing high-performance devices, such as light-emitting diodes (LEDs), photodetectors, lasers, and optical cavities as well as others [25], [26]. The first generation of 2D phototransistors demonstrated photo responsivity on the order of about 120 mA/W despite being severely limited by contact resistance [27]. This issue was

shown to be resolvable through low contact resistance monolayer WSe_2 phototransistors, which exhibited photo responsivity as high as ~1.8×10^5 A/W [28]. Finally, when high mobility graphene was combined with MoS_2 in hybrid graphene–MoS_2 phototransistor, the photo responsivity was recorded to be even higher at about 5×10^8 A/W under high room temperature [29]. Other device architectures also exist involving TMDCs. One of these is WSe_2 p–n photodiodes with two local bottom gates having different gate dielectrics. This device has shown photo detection responses up to 320 mA/W, which is comparable to state-of-the-art commercial silicon photodetectors. Other examples include solar cells or photodetectors, where significant absorption of large fractions of light is necessary. This can be a concern for atomically thick materials. To remedy this, simple architectures such as those based on the "Salisbury screen" concept have been proposed. These consist of placing the 2D material a quarter wavelength from a reflecting ground plane. Optical cavities can also support a perfect absorption even for monolayer thicknesses but only in a narrow wavelength band defined by a Fabry–Perot resonance [30]. More broadband enhancement of light absorption in ultrathin films is also possible in plasmonic or dielectric gap-mode architectures [31].

In search of other strong photo detection and multifunctional devices, this work focuses on more exotic materials, such as alloys and those that possess a CDW phase. CDW is a ground state with a periodic modulation of charge density associated with a periodic distortion of the crystal lattice [32], [33]. The transition to the CDW state is usually depicted as the consequence of Fermi surface nesting with a wave vector $Q = 2k_F$ and exhibits an energy gap at the Fermi energy [34]. For instance, a widely studied CDW material is the quasi-1D material $NbSe_3$

which exhibits two CDW transitions. The first transition forms at T_{p1} = 145 K and removes roughly half the total metallic carrier density with $n_s = 3.8 \times 10^{21}$ cm^{-3}. The second transition forms at T_{p2} = 59 K, leaving a small part of the Fermi surface with $n_s = 6 \times 10^{18}$ cm^{-3} ungapped so that the low-field conduction remains metallic at low temperatures [33]. Alloys such as layered Janus MoSSe have recently been synthesized and are under investigation. Janus is a nano- or micro-sized material with two or more distinct surface properties. One of the S layers within MoS_2 is replaced by Se atoms at an appropriate temperature. This is accomplished mainly through a chemical vapor deposition (CVD) method [35]. The alloyed MoSSe not only inherits some properties of MoS_2, but can create other properties like appealing new mechanisms for light–electricity conversion [36]. Additionally, the material also possesses advantages over MoS_2 in terms of interior electric field and tunable selectivity originating from the Janus structure [37]. The Se atoms in Janus MoSSe will cause different adsorption behaviors of gas molecules on both sides of Janus MoSSe, which leads to distinct electronic properties. These properties raised promising prospects for developing new Janus MoSSe-based ultrahigh-sensitivity devices [38]. Based on the properties of the components, alloyed materials could show stronger or unique properties which may help nanodevice engineering. This work focuses on exploring the optical, electrical, and optoelectronic properties of the alloyed 2D material $TaWSe_2$.

Chapter II. Background

1. Related works of $TaSe_2$

$TaWSe_2$ is the ternary alloy of $TaSe_2$ and WSe_2. As a newly synthesized material, most properties are unknown. Since alloys of 2D materials may inherit the properties of their component [39], we review the properties of $TaSe_2$ and WSe_2 here to anticipate the properties and motivate the study of $TaWSe_2$.

2H tantalum diselenide (2H-$TaSe_2$) is a TMDC that has shown metallic properties and promise as a contact material for nanoelectronic devices [40], [41]. 2H-$TaSe_2$ is a great choice as a contact material since it exhibits both strong electron-phonon coupling and spin-orbit coupling, both of which can play a significant role in charge density wave (CDW) transport properties [42]. The band structure of 2H-$TaSe_2$ shows a narrow band around the Fermi energy with uniquely structured Fermi surfaces. Furthermore, there is a large gap above and below the bands around the Fermi energy in the normal metal phase. This is expected to have potential for strong optical properties [43]. With excellent electrical transport and optical properties coupled with the possibility of wafer-scale growth [44], 2H-$TaSe_2$ can be a potential material for optoelectronic applications.

Hajiyev et al have reported the successful preparation of single and few-layer 2H-$TaSe_2$ by mechanical exfoliation techniques and shown thickness dependent properties [45]. The number of layers is confirmed by white light contrast spectroscopy and atomic force microscopy (AFM) in their work. Vibrational properties of the atomically thin layers of 2H-$TaSe_2$ are characterized by micro-Raman spectroscopy. Their Raman data is shown in Fig. 1.

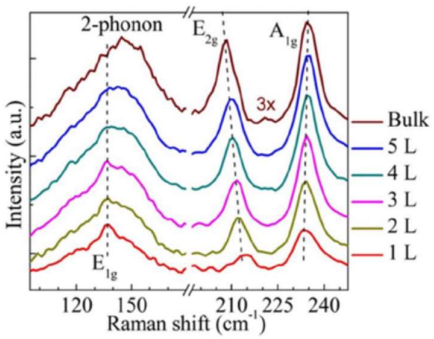

Figure. 1 Raman spectra of $TaSe_2$ layer samples, ranging from single layer to bulk at room temperature, reprinted with permissions from [45]. Copyright © 2013, *Scientific reports*

There are three prominent Raman peaks shown in Fig. 1. These are the A_{1g} peak around 235cm^{-1}, E_{2g} peak around 212cm^{-1}, and the 2-phonon mode for $TaSe_2$ samples ranging from single layer to bulk. It can be observed from Fig. 1 that the intensity of the E_{1g} mode increases with the decreasing number of layers. The E_{1g} peak of the thicker layers does not appear as clearly as it does in the thinner layers, this could be caused by (i) the second order Raman peak intensity grows with the number of layers, which may "suppress" the very weak E_{1g} peak; (ii) the interaction of thicker layers and the substrate could be dramatically weaker compared to the case for very thin layers, this may further weaken the E_{1g} intensity. Analogous to MoS_2, A_{1g} and E_{2g} peaks approach each other as the number of layers decreases [10], [11]. From bulk to single layer, the E_{2g} mode presents a blue-shift of 6.5 cm^{-1}. These shifts are mainly attributed to: (i) the decrease of the force constant resulted from the weakening of the interlayer Van der Waals (vdW) force between layers for the A_{1g} mode [46]; (ii) the structure changes or long-range coulombic interlayer interactions for the E_{2g} mode when the number of layers decreases [47].

2. Related works of WSe_2

Tungsten diselenide (WSe_2) is a semiconductor that exhibits both electron and hole conduction with relatively high carrier mobility [48], strong optical absorption and high photo-conversion efficiency [9], [49]. Suppression or enhancement of one of the two conduction branches can be effectively obtained by exploiting electrostatic doping [50], [51]. This is a unique property among TMDCs given that they are typically unipolar with dominant electron conduction. WSe_2 becomes one of the best choices for the realization of a single material for optoelectronic applications. When WSe_2 is scaled down from the bulk to the monolayer form, it shows strong photoluminescence possibly due to the quantum confinement effect [52]. Furthermore, the internal quantum efficiency of WSe_2 is more than 70%, which is much higher than other TMDCs [53]. These properties strongly indicate that WSe_2 is an ideal material for optoelectronic devices such as photodetectors and light-emitting diodes [9], [26], [54].

Zeng et al reported optical studies in WSe_2 multilayers[55]. Fig. 2 presents representative Raman spectra of WSe_2 with the layer numbers from 1 to 4 and in bulk. Two dominant peaks are observed around 250 cm^{-1} in various samples from monolayer to bulk. In their study, photoluminescence shows that similar to MoS_2, WSe_2 exhibits a transition from indirect bandgap semiconductor in the bulk and multilayer form to direct bandgap in the monolayers form [56].

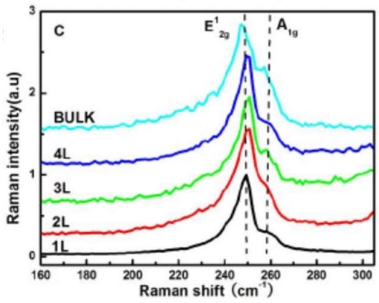

Figure. 2 Raman spectra of WSe_2 layer samples, ranging from single layer to bulk at room temperature, reprinted with permissions from [55]. Copyright © 2013, *Scientific reports*

Chapter III. Materials and Methods

1. $TaWSe_2$ Synthesis

$TaWSe_2$ Crystals were synthesized by the *2D Semiconductors*. The crystals used in this study are layered $TaWSe_2$ ternary alloys that have been synthesized at 50%-50% W (tungsten) to Ta (tantalum) ratios. A flux zone technique was used to produce high-quality crystals with strong atomic structuring and nearly impurity-free growth with low defect concentrations.

2. $TaWSe_2$ device Fabrication

Adhesive tape was used to split $TaWSe_2$ bulk crystals. Achieving few-layer samples typically require multiple exfoliation steps, each producing a slice with fewer layers. Then the $TaWSe_2$ flakes were exfoliated onto a silicon/silicon dioxide wafer.

After obtaining an appropriate flake, the next step is to attach electrodes. First, gold electrodes were prepared on a sacrificial silicon substrate using standard photolithography and deposition procedures. The electrodes are then processed with hexamethyldisilazane (HMDS) and coated with a thick layer of Polymethyl methacrylate (PMMA). Second, a polydimethylsiloxane (PDMS) stamp is needed to transfer the electrodes. This was created from a Silicone Elastomer Curing Agent and Silicone Elastomer Base at 1 to 10 ratios. Next, the electrodes were picked up with the PDMS stamp on a slide. The PDMS stamp with the electrodes was aligned and slowly placed on the silicon/silicon dioxide wafer surface containing the flake. After contact is attained, the substrate was heated for 5 minutes to peel the PDMS stamp off and leave behind the PMMA/gold electrode structure. The electrodes

picked up by the PDMS will be left on the silicon/silicon dioxide wafer. This technique was developed by Liu et al [57].

Contact pads of the transferred electrodes are opened by electron beam lithography (EBL) then cut into smaller pieces to fit inside a chip carrier and wire bound. Fig. 3 demonstrates the optical image of the fabricated $TaWSe_2$ device using a 100x objective.

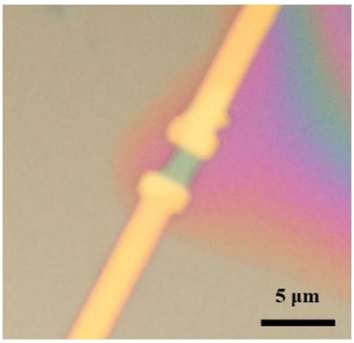

Figure. 3 Optical micrograph of fabricated $TaWSe_2$ phototransistor device.

3. Electrical and Optoelectronic Measurement

An Olympus microscopy setup was used to measure the electrical and optoelectronic properties of the $TaWSe_2$ device. Fig. 4 shows the schematic of the measurement system. A continuous wave laser beam (NKT Photonics SuperK Supercontinuum Laser) is expanded and focused with a 40x objective to scan over the device. Current is collected via a DL instrument current preamplifier. Additionally, photocurrent signals are collected as a function of position simultaneously with a reflection image by a photodetector. Experiments on the device are performed in a Janis ST-500 microscopy cryostat under a high vacuum environment.

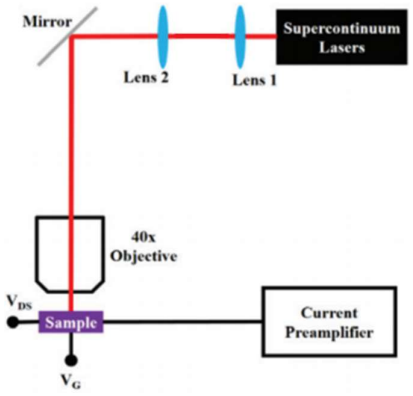

Figure. 4 Schematic of the setup used to perform photocurrent measurements, reprinted with permissions from [58]. Copyright © 2019, *Nanoscale*

Chapter IV. Results and Discussion

1. Raman and AFM data of $TaWSe_2$ Device

The $TaWSe_2$ few-layer device was identified by optical microscopy and characterized with a Bruker Dimension Icon AFM and a Thermo Scientific DXR Raman 532nm microscope. The measurements were obtained in the Vanderbilt Institute for Nanoscale Science and Engineering (VINSE) imaging core and analytical lab. Fig. 5 shows optical images of $TaWSe_2$ flakes under 100x magnification. (Fig. 5a to 5c), AFM images (Fig. 5d to 5f) and cutline images of the flakes (Fig. 5g to 5i). Cutline images show a similar thickness of the $TaWSe_2$ flakes used for the device, around 85 nm to 90nm.

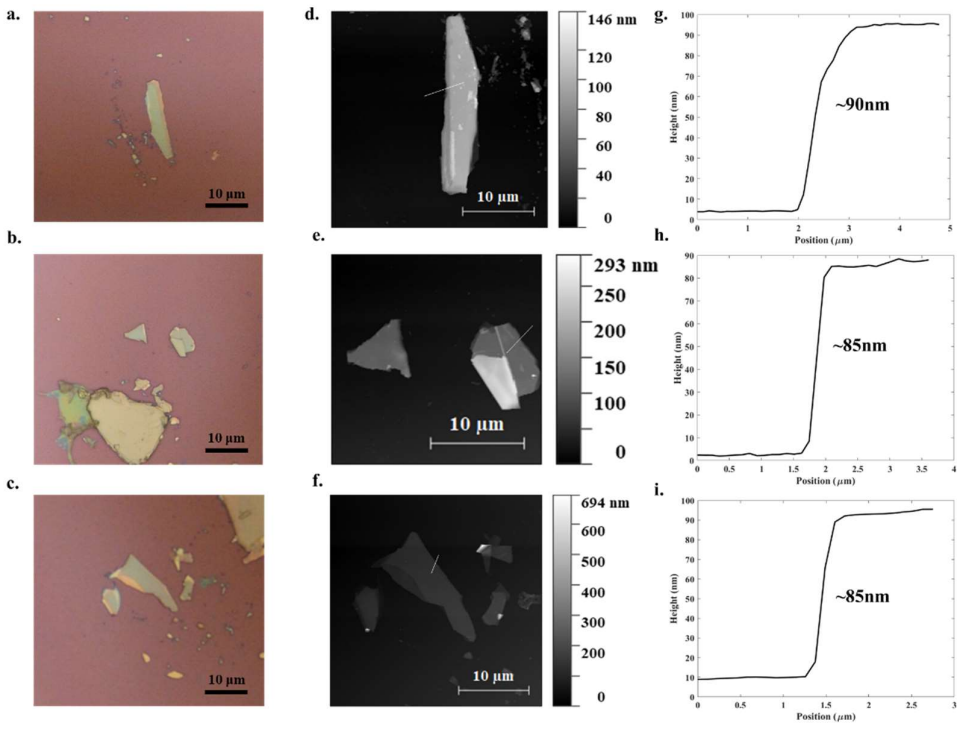

Figure. 5 (a to c) Optical images of exfoliated $TaWSe_2$ flakes. (d to f) AFM topography images of exfoliated $TaWSe_2$ flakes. The white line indicated the cutline used to extract the flake thickness. (g to i) Height profiles for the cutline in the AFM topography image.

Fig. 6d to 6f present the Raman spectra data of the same $TaWSe_2$ flakes. From these measurements, $TaWSe_2$ appears to have three dominant Raman peaks. The first peak is around 104 cm^{-1}, the second is around 240 cm^{-1} and the third is around 305 cm^{-1}. As was mentioned in Chapter I, some alloys of 2D material inherit the properties of its component. We can find that both WSe_2 and $TaSe_2$ have a Raman peak around 240 cm^{-1}, which may correspond to the Raman peak of $TaWSe_2$. Furthermore, two unknown peaks around 305 cm^{-1} and 105 cm^{-1} require further theoretical calculations to identify the nature of these vibrational modes.

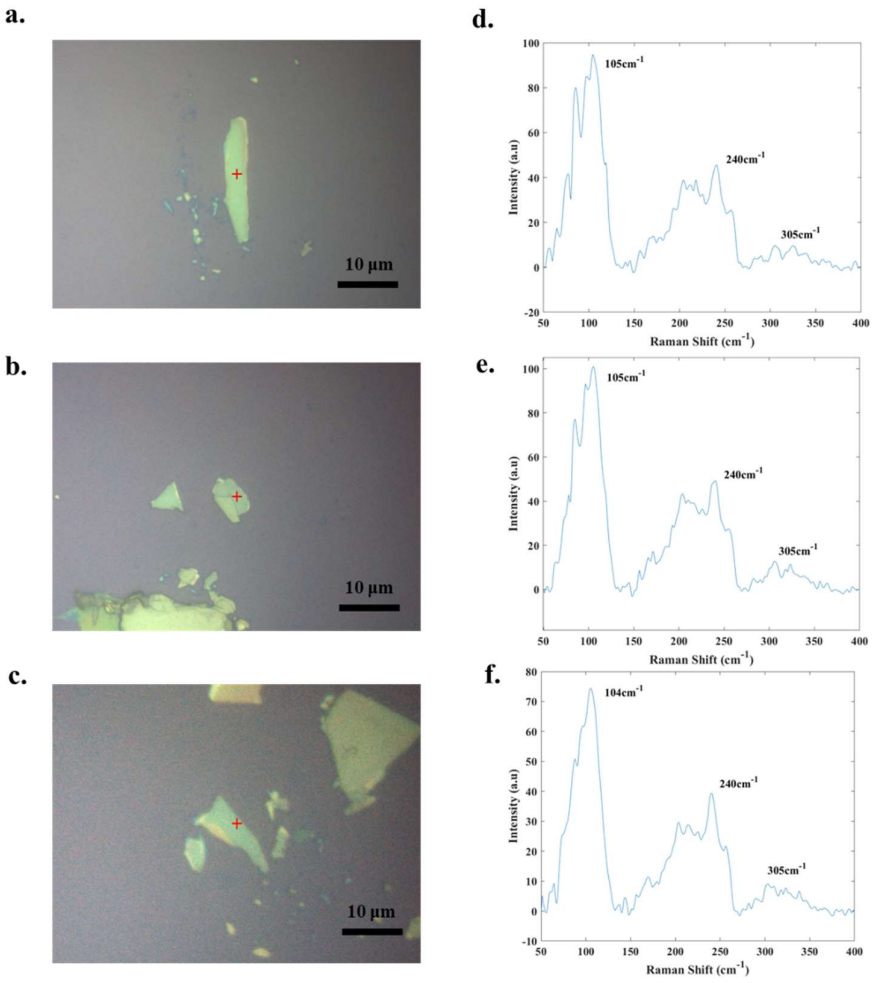

Figure. 6 Optical image of $TaWSe_2$ flakes used for measurement (a to c) and Raman spectra of the flakes (d to f).

2. Electrical and Optoelectronic Properties of $TaWSe_2$ Device

An Olympus microscopy setup is used to perform photocurrent measurement to characterize the photoresponse properties of the $TaWSe_2$ device. Fig. 7 shows the scanning photocurrent image and the simultaneously recorded reflection image of the $TaWSe_2$ device under 1064nm wavelength illumination. The electrodes and $TaWSe_2$ flake are outlined by grey and red lines, respectively. Photocurrent responses ($I_{pc} = I_{laser} - I_{dark}$) are observed in red and blue. Strong photocurrent responses observed at the $TaWSe_2$-metal junction are possibly due to the creation of Schottky-like barriers that result in built-in electric fields which can efficiently separate photo-excited electron-hole pairs (EHPs) [59].

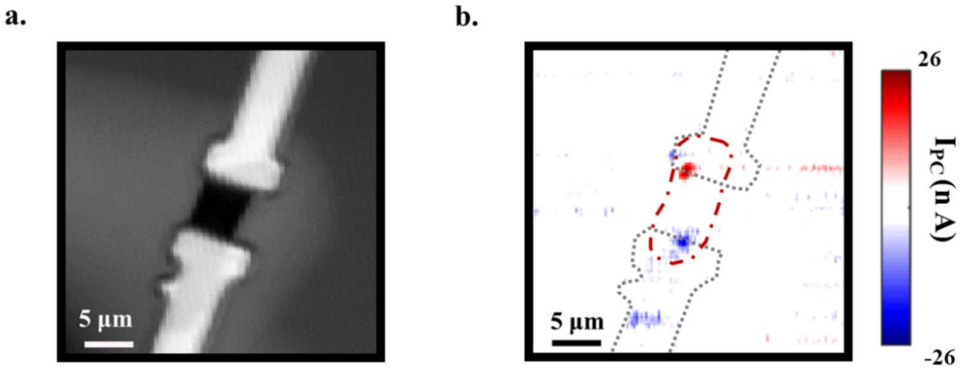

Figure. 7 Reflection (a) and scanning (b) photocurrent images of the $TaWSe_2$ device with zero drain-source bias under 1064nm laser. Grey and red lines represent the electrodes and $TaWSe_2$ flake.

Furthermore, power dependent measurements are performed on the $TaWSe_2$ device. As shown in Fig. 8a, the photocurrent signals present a nearly linear relationship. Since the number of incident photons increases with increasing power, there is also an expected increase in the number of EHPs, which should result in a linear behavior. The observed deviations from the expected linear behavior may be caused by some defects [60].

Moreover, temperature dependent measurements are taken to characterize the phase transition of the $TaWSe_2$ device. Fig. 8b displays temperature dependent resistance measurements of the $TaWSe_2$ device. Temperature dependent resistance measurements can be used to show phase transitions. In 2H-$TaSe_2$ a slight change in slope indicates a phase transition [40], [61]. Examining these measurements for the $TaWSe_2$ device, a slight change in slope can be seen at around 190K (the fit line below 190K is 0.31 Ω/K, the fit line above 190K is 0.65 Ω/K). It may present a new phase transition property as the measurements on $TaSe_2$ or WSe_2 have not performed phase transition at 190K. Further experiments are required to identify the characteristic. Additionally, the decrease in resistance with temperature suggests a metallic nature of $TaWSe_2$ possibly due to the reduction in scattering from thermally activated carriers [40], [41].

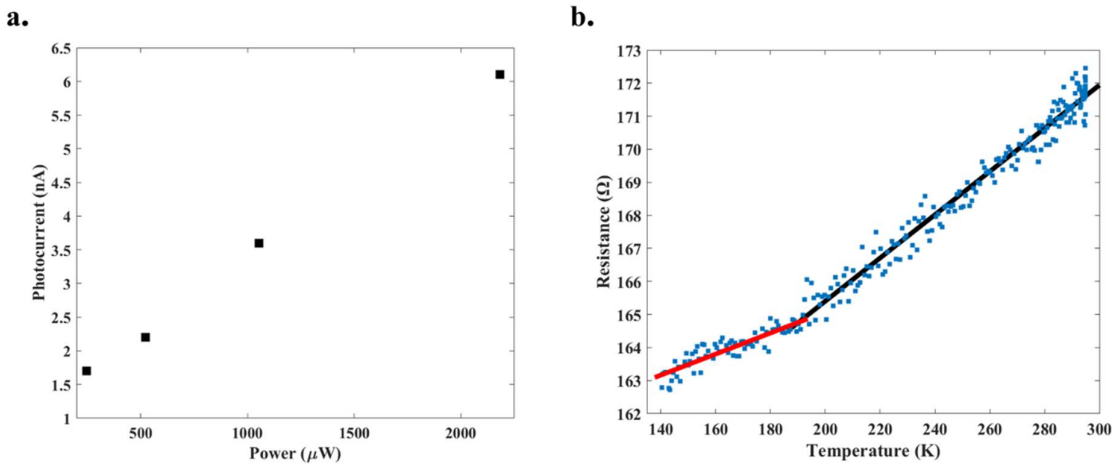

Figure. 8 (a) Power dependent photocurrent response of $TaWSe_2$ device. (b) Output property of $TaWSe_2$ device at different temperatures. The red and black lines in the figure correspond to the fitting lines of the data from 140 K to 190 K and the data from 190 K to 295 K, respectively. The slope of the red line is 0.31 and the slope of the black line is 0.65.

Chapter V. Conclusion

In this work, a $TaWSe_2$ crystal is exfoliated into few layers and then fabricated into an optoelectronic device. This new ternary alloy has not been previously investigated in its bulk or few-layer form. First, optical investigations show that few-layer $TaWSe_2$ flakes have similar Raman signatures to WSe_2 and 2H-$TaSe_2$ and may have similar vibrations modes. Second, through scanning photocurrent microscopy, optoelectronic properties of $TaWSe_2$ device reveal strong photocurrent responses at the $TaWSe_2$-metal junction with nearly linear photocurrent-power dependence. Finally, electrical measurements show temperature dependent resistance properties of the $TaWSe_2$ device suggesting metallic characteristics and potentially a phase transition. In conclusion, this work presents that TaWSe2 alloys may inherit properties from its component and show a solid potential for apply alloyed 2D materials in optoelectronic devices.

REFERENCES

[1] B.C. Brodie, “On the Atomic Weight of Graphite Author (s): B . C . Brodie Source : Philosophical Transactions of the Royal Society of London , Vol . 149 (1859), pp . 249- Published by : Royal Society Stable URL : http://www.jstor.org/stable/108699 Accessed : 27-04-,” *Philos. Trans. R. Scociety London*, vol. 149, no. 1859, pp. 249–259, 1859.

[2] A. A. Firsov *et al.*, “Electric field effect in atomically thin carbon films.,” *Sci. (New York, NY)*, 2004.

[3] A. K. Geim and K. S. Novoselov, “The rise of graphene,” in *Nanoscience and technology: a collection of reviews from nature journals*, World Scientific, 2010, pp. 11–19.

[4] F. Bonaccorso, Z. Sun, T. A. Hasan, and A. C. Ferrari, “Graphene photonics and optoelectronics,” *Nat. Photonics*, vol. 4, no. 9, p. 611, 2010.

[5] L. Britnell *et al.*, “Resonant tunnelling and negative differential conductance in graphene transistors,” *Nat. Commun.*, vol. 4, no. 1, pp. 1–5, 2013.

[6] Y.-M. Lin *et al.*, “100-GHz transistors from wafer-scale epitaxial graphene,” *Science (80-.).*, vol. 327, no. 5966, p. 662, 2010.

[7] Q. H. Wang, K. Kalantar-Zadeh, A. Kis, J. N. Coleman, and M. S. Strano, “Electronics and optoelectronics of two-dimensional transition metal dichalcogenides,” *Nat. Nanotechnol.*, vol. 7, no. 11, pp. 699–712, 2012.

[8] K. F. Mak, K. He, J. Shan, and T. F. Heinz, “Control of valley polarization in monolayer MoS 2 by optical helicity,” *Nat. Nanotechnol.*, vol. 7, no. 8, pp. 494–498, 2012.

[9] J. S. Ross *et al.*, “Electrically tunable excitonic light-emitting diodes based on monolayer WSe 2 p–n junctions,” *Nat. Nanotechnol.*, vol. 9, no. 4, pp. 268–272, 2014.

[10] A. Splendiani *et al.*, “Emerging photoluminescence in monolayer MoS2,” *Nano Lett.*, vol. 10, no. 4, pp. 1271–1275, 2010.

[11] K. F. Mak, C. Lee, J. Hone, J. Shan, and T. F. Heinz, “Atomically thin MoS 2: a new direct-gap semiconductor,” *Phys. Rev. Lett.*, vol. 105, no. 13, p. 136805, 2010.

[12] D. Xiao, G.-B. Liu, W. Feng, X. Xu, and W. Yao, “Coupled spin and valley physics in monolayers of MoS 2 and other group-VI dichalcogenides,” *Phys. Rev. Lett.*, vol. 108, no. 19, p. 196802, 2012.

[13] A. J. Mannix *et al.*, “Synthesis of borophenes: Anisotropic, two-dimensional boron polymorphs,” *Science (80-.).*, vol. 350, no. 6267, pp. 1513–1516, 2015.

[14] Y. Shi *et al.*, “Synthesis of few-layer hexagonal boron nitride thin film by chemical vapor deposition,” *Nano Lett.*, vol. 10, no. 10, pp. 4134–4139, 2010.

[15] L. Li *et al.*, “Black phosphorus field-effect transistors,” *Nat. Nanotechnol.*, vol. 9, no. 5, p. 372, 2014.

[16] J. Qiao, X. Kong, Z.-X. Hu, F. Yang, and W. Ji, “High-mobility transport anisotropy and linear dichroism in few-layer black phosphorus,” *Nat. Commun.*, vol. 5, no. 1, pp. 1–7, 2014.

[17] K. Zhang, Y. Feng, F. Wang, Z. Yang, and J. Wang, “Two dimensional hexagonal boron nitride (2D-hBN): synthesis, properties and applications,” *J. Mater. Chem. C*, vol. 5, no. 46, pp. 11992–12022, 2017.

[18] V. Tran, R. Soklaski, Y. Liang, and L. Yang, “Layer-controlled band gap and anisotropic excitons in few-

layer black phosphorus," *Phys. Rev. B*, vol. 89, no. 23, p. 235319, 2014.

[19] G. Long *et al.*, "Achieving ultrahigh carrier mobility in two-dimensional hole gas of black phosphorus," *Nano Lett.*, vol. 16, no. 12, pp. 7768–7773, 2016.

[20] F. Xia, H. Wang, and Y. Jia, "Rediscovering black phosphorus as an anisotropic layered material for optoelectronics and electronics," *Nat. Commun.*, vol. 5, no. 1, pp. 1–6, 2014.

[21] Z. Zhang, Y. Yang, E. S. Penev, and B. I. Yakobson, "Elasticity, flexibility, and ideal strength of borophenes," *Adv. Funct. Mater.*, vol. 27, no. 9, p. 1605059, 2017.

[22] B. Peng, H. Zhang, H. Shao, Y. Xu, R. Zhang, and H. Zhu, "The electronic, optical, and thermodynamic properties of borophene from first-principles calculations," *J. Mater. Chem. C*, vol. 4, no. 16, pp. 3592–3598, 2016.

[23] M. Novotný, F. J. Domínguez-Gutiérrez, and P. Krstić, "A computational study of hydrogen detection by borophene," *J. Mater. Chem. C*, vol. 5, no. 22, pp. 5426–5433, 2017.

[24] M. Osada and T. Sasaki, "Two-dimensional dielectric nanosheets: novel nanoelectronics from nanocrystal building blocks," *Adv. Mater.*, vol. 24, no. 2, pp. 210–228, 2012.

[25] W. J. Yu *et al.*, "Highly efficient gate-tunable photocurrent generation in vertical heterostructures of layered materials," *Nat. Nanotechnol.*, vol. 8, no. 12, pp. 952–958, 2013.

[26] B. W. H. Baugher, H. O. H. Churchill, Y. Yang, and P. Jarillo-Herrero, "Optoelectronic devices based on electrically tunable p–n diodes in a monolayer dichalcogenide," *Nat. Nanotechnol.*, vol. 9, no. 4, pp. 262–267, 2014.

[27] O. Lopez-Sanchez, D. Lembke, M. Kayci, A. Radenovic, and A. Kis, "Ultrasensitive photodetectors based on monolayer MoS 2," *Nat. Nanotechnol.*, vol. 8, no. 7, pp. 497–501, 2013.

[28] W. Zhang, M.-H. Chiu, C.-H. Chen, W. Chen, L.-J. Li, and A. T. S. Wee, "Role of metal contacts in high-performance phototransistors based on WSe2 monolayers," *ACS Nano*, vol. 8, no. 8, pp. 8653–8661, 2014.

[29] K. Roy *et al.*, "Graphene–MoS 2 hybrid structures for multifunctional photoresponsive memory devices," *Nat. Nanotechnol.*, vol. 8, no. 11, pp. 826–830, 2013.

[30] M. S. Jang *et al.*, "Tunable large resonant absorption in a midinfrared graphene Salisbury screen," *Phys. Rev. B*, vol. 90, no. 16, p. 165409, 2014.

[31] Z. Yu, A. Raman, and S. Fan, "Fundamental limit of nanophotonic light trapping in solar cells," *Proc. Natl. Acad. Sci.*, vol. 107, no. 41, pp. 17491–17496, 2010.

[32] G. Grüner, "The dynamics of charge-density waves," *Rev. Mod. Phys.*, vol. 60, no. 4, p. 1129, 1988.

[33] T. L. Adelman, S. V Zaitsev-Zotov, and R. E. Thorne, "Field-effect modulation of charge-density-wave transport in NbSe 3 and TaS 3," *Phys. Rev. Lett.*, vol. 74, no. 26, p. 5264, 1995.

[34] M. Bovet *et al.*, "Pseudogapped Fermi surfaces of 1 T− TaS 2 and 1 T− TaSe 2: A charge density wave effect," *Phys. Rev. B*, vol. 69, no. 12, p. 125117, 2004.

[35] A.-Y. Lu *et al.*, "Janus monolayers of transition metal dichalcogenides," *Nat. Nanotechnol.*, vol. 12, no. 8, pp. 744–749, 2017.

[36] F. Li, W. Wei, H. Wang, B. Huang, Y. Dai, and T. Jacob, "Intrinsic electric field-induced properties in Janus MoSSe van der Waals structures," *J. Phys. Chem. Lett.*, vol. 10, no. 3, pp. 559–565, 2019.

[37] Q. Yue, Z. Shao, S. Chang, and J. Li, "Adsorption of gas molecules on monolayer MoS 2 and effect of applied electric field," *Nanoscale Res. Lett.*, vol. 8, no. 1, pp. 1–7, 2013.

[38] C. Jin, X. Tang, X. Tan, S. C. Smith, Y. Dai, and L. Kou, "A Janus MoSSe monolayer: a superior and strain-sensitive gas sensing material," *J. Mater. Chem. A*, vol. 7, no. 3, pp. 1099–1106, 2019.

[39] R. Venkatasubramanian, E. Siivola, T. Colpitts, and B. O'quinn, "Thin-film thermoelectric devices with high room-temperature figures of merit," *Nature*, vol. 413, no. 6856, pp. 597–602, 2001.

[40] A. T. Neal, Y. Du, H. Liu, and P. D. Ye, "Two-dimensional TaSe2 metallic crystals: spin–orbit scattering length and breakdown current density," *ACS Nano*, vol. 8, no. 9, pp. 9137–9142, 2014.

[41] M. Naito and S. Tanaka, "Electrical transport properties in 2H-," *J. Phys. Soc. Japan*, vol. 51, no. 1, p. 219, 1982.

[42] K. Rossnagel and N. V Smith, "Spin-orbit splitting, Fermi surface topology, and charge-density-wave gapping in 2 H− Ta Se 2," *Phys. Rev. B*, vol. 76, no. 7, p. 73102, 2007.

[43] Y. W. Li *et al.*, "Folded superstructure and degeneracy-enhanced band gap in the weak-coupling charge density wave system 2 H− TaSe 2," *Phys. Rev. B*, vol. 97, no. 11, p. 115118, 2018.

[44] J. Shi *et al.*, "Chemical Vapor Deposition Grown Wafer-Scale 2D Tantalum Diselenide with Robust Charge-Density-Wave Order," *Adv. Mater.*, vol. 30, no. 44, p. 1804616, 2018.

[45] P. Hajiyev, C. Cong, C. Qiu, and T. Yu, "Contrast and Raman spectroscopy study of single-and few-layered charge density wave material: 2H-TaSe 2," *Sci. Rep.*, vol. 3, no. 1, pp. 1–6, 2013.

[46] H. Li *et al.*, "From bulk to monolayer MoS2: evolution of Raman scattering," *Adv. Funct. Mater.*, vol. 22, no. 7, pp. 1385–1390, 2012.

[47] C. Lee, H. Yan, L. E. Brus, T. F. Heinz, J. Hone, and S. Ryu, "Anomalous lattice vibrations of single-and few-layer MoS2," *ACS Nano*, vol. 4, no. 5, pp. 2695–2700, 2010.

[48] A. Allain and A. Kis, "Electron and hole mobilities in single-layer WSe2," *ACS Nano*, vol. 8, no. 7, pp. 7180–7185, 2014.

[49] Y. V Morozov and M. Kuno, "Optical constants and dynamic conductivities of single layer MoS2, MoSe2, and WSe2," *Appl. Phys. Lett.*, vol. 107, no. 8, p. 83103, 2015.

[50] N. Oliva, E. A. Casu, M. Cavalieri, and A. M. Ionescu, "Double gate n-type WSe2 FETs with high-k top gate dielectric and enhanced electrostatic control," in *2018 48th European Solid-State Device Research Conference (ESSDERC)*, 2018, pp. 114–117.

[51] G. V Resta *et al.*, "Polarity control in WSe 2 double-gate transistors," *Sci. Rep.*, vol. 6, no. 1, pp. 1–6, 2016.

[52] W. Zhao *et al.*, "Evolution of electronic structure in atomically thin sheets of WS2 and WSe2," *ACS Nano*, vol. 7, no. 1, pp. 791–797, 2013.

[53] M. Massicotte *et al.*, "Picosecond photoresponse in van der Waals heterostructures," *Nat. Nanotechnol.*, vol. 11, no. 1, pp. 42–46, 2016.

[54] Z. Zheng, T. Zhang, J. Yao, Y. Zhang, J. Xu, and G. Yang, "Flexible, transparent and ultra-broadband photodetector based on large-area WSe2 film for wearable devices," *Nanotechnology*, vol. 27, no. 22, p. 225501, 2016.

[55] H. Zeng *et al.*, “Optical signature of symmetry variations and spin-valley coupling in atomically thin tungsten dichalcogenides,” *Sci. Rep.*, vol. 3, no. 1, pp. 1–5, 2013.

[56] S. Lebegue and O. Eriksson, “Electronic structure of two-dimensional crystals from ab initio theory,” *Phys. Rev. B*, vol. 79, no. 11, p. 115409, 2009.

[57] Y. Liu *et al.*, “Approaching the Schottky–Mott limit in van der Waals metal–semiconductor junctions,” *Nature*, vol. 557, no. 7707, pp. 696–700, 2018.

[58] T. S. Walmsley *et al.*, “Near-infrared optical transitions in PdSe 2 phototransistors,” *Nanoscale*, vol. 11, no. 30, pp. 14410–14416, 2019.

[59] T. Hong *et al.*, “Polarized photocurrent response in black phosphorus field-effect transistors,” *Nanoscale*, vol. 6, no. 15, pp. 8978–8983, 2014.

[60] O. Lopez-Sanchez, D. Lembke, and M. Kayci, “Radenovic, & A. Kis, A,” *Ultrasensitive photodetectors based monolayer MoS2. Nat. Nanotechnol*, vol. 8, pp. 497–501, 2013.

[61] H. N. S. Lee, M. Garcia, H. McKinzie, and A. Wold, “The low-temperature electrical and magnetic properties of TaSe2 and NbSe2,” *J. Solid State Chem.*, vol. 1, no. 2, pp. 190–194, 1970.